Mechanism of magnesium transport in spinel chalcogenides

Mohsen Sotoudeh
Ulm University https://orcid.org/0000-0002-0970-5336
Manuel Dillenz
Ulm University
Axel Groß (axel.gross@uni-ulm.de)
Ulm University https://orcid.org/0000-0003-4037-7331

Research Article

Keywords: ion conductivity, density functional theory, magnesium batteries, ternary spinel chalcogenides

Posted Date: May 17th, 2021

DOI: https://doi.org/10.21203/rs.3.rs-358467/v2

Version of Record: A version of this preprint was published at Advanced Energy and Sustainability Research on August 4th, 2021. See the published version at https://doi.org/10.1002/aesr.202100113.

Mechanism of magnesium transport in spinel chalcogenides

Mohsen Sotoudeh,[†] Manuel Dillenz,[†] and Axel Groß[*,†,‡]

[†]*Institute of Theoretical Chemistry, Ulm University, Albert-Einstein-Allee 11, 89081 Ulm, Germany*

[‡]*Helmholtz Institute Ulm (HIU) for Electrochemical Energy Storage, Helmholtzstraße 11, 89069 Ulm, Germany*

E-mail: axel.gross@uni-ulm.de

Abstract

In the area of sustainable energy storage, batteries based on multivalent ions such as magnesium have been attracting considerable attention due to their potential for high energy densities. Furthermore, they are typically also more abundant than, e.g., lithium. However, as a challenge their low ion mobility in electrode materials remains. This study addresses the ionic conductivity in spinel host materials which represent a promising class of cathode and solid-electrolyte materials in Mg-ion batteries. Based on periodic density functional theory calculations, we identify the critical parameters which determine the mobility and insertion of ions. We will in particular highlight the critical role that trigonal distortions of the spinel structure play for the ion mobility. In detail, we will show that it is the competition between coordination and bond length that governs the Mg site preference in ternary spinel compounds upon trigonal distortions. This can only be understood by also taking covalent interactions into account. Furthermore, our calculations suggest that anionic redox plays a much more important role in sulfide and selenide spinels than in oxide spinels. Based on our theoretical study, we rationalize the impact of the metal distribution in the host material and the ion concentration on the diffusion process. Furthermore, cathode-related challenges for practical devices will be addressed. Our findings shed light on the fundamentional mechanisms underlying ionic conductivity in solid hosts and thus may contribute to improve ion transport in battery electrodes.

Introduction

The development of Li-ion batteries (LIBs) had a major impact on the wide-spread use of portable electronic devices. However, there are safety and abundance issues associated with LIBs[1,2] that motivate the search for alternative battery chemistries.[3,4] As a promising alternative, magnesium has been proposed[5–8] as an active element with a much higher earth-abundance of 13.9% compared to 7×10^{-4}% of Li. The ionic radii of Mg^{2+}, 0.86 Å and Li^{+}, 0.90 Å are rather similar,[1] but Mg has the advantage of being a bivalent ion which

leads to a higher volumetric capacity of Mg metal anodes compared to Li, 3833 $mAhcm^{-3}$ vs 2062 $mAhcm^{-3}$, and also to a low reduction potential of -2.37 V vs SHE compared to -3.05 V of Li .[9,10] Furthermore, Mg-ion batteries (MIBs) exhibit a low tendency for dendrite formation[11–15] and a high melting point.

A high multi-valent ionic conductivity of 1-10 mS cm^{-1} has been achieved in MIBs at high temperatures .[16,17] However, a major problem for MIBs lies in the sluggish kinetics during intercalation at room temperature.[2,18] It should be noted that the design of chemically stable electrodes with high ionic conductivity is highly desirable,[2,19–23] as a low ionic mobility can severely limit the performance of batteries.

In order to address the slow migration of Mg-ion in cathode materials at low temperatures, Chevrel phases and layered and spinel TiS_2 structures have been studied in detail.[24] A Mg-ion migration barrier of about 550 meV was found in cubic Ti_2S_4 using galvanostatic intermittent titration technique measurements. Studies on the sulfide and selenide spinel frameworks indicate low energy barriers for Mg-ion diffusion comparable to those of LIBs.[25] In contrast, oxide spinel cathode materials exhibit high migration barriers for Mg-ions which is caused by the relatively strong Coulombic attraction between the guest Mg^{2+} and host oxygen lattice[23] which leads to a lower ion mobility. The smaller electronegativity of sulfur and selenium lattices enlarges the lattice constant of these materials and thus also their ion mobility as typically diffusion barriers become smaller for larger lattice constants. Nevertheless, the increase of the ion mobility through the lowering of diffusion barriers is also accompanied by lower Mg insertion energies into the spinel structures which lowers the voltage[26,27] and thus causes a reduction of the energy densities of chalcogenide materials.

Recently, $MgSc_2Se_4$ has been found to be a super-ionic conductor exhibiting a high Mg-ion conductivity of 0.1 $mScm^{-1}$ at room temperature.[25] This high ion mobility does not only make $MgSc_2Se_4$ to a promising cathode material for MIBs, it also suggests that it could be used as a solid electrolyte. However, solid electrolytes need to exhibit a very low electronic conductivity whereas $MgSc_2Se_4$ is also a good electron conductor.

Doping $MgSc_2Se_4$ by Ti and Ce leading to Ti^{4+}- and Ce^{4+} impurities, respectively, has been considered as a means to lower and neutralize the electronic conductivity.[22] Still, a high electron conductivity has been observed in these materials which has been related to the presence of defects or the phase deformation.[25,28] Furthermore, it has been shown that for chalcogenide spinels containing lanthanoids the Mg mobility increases with the size of the lanthanoids.[29]

Note that spinel structures including transition metal ions such as Ti, Mn, Fe and Co exhibit magnetic properties due to the filling of the $3d$ shell which cause significant distortions of the crystal lattice, namely trigonal distortion, as we will show below. Such trigonal distortions have hardly been considered in determining the transport properties of sulfide and selenide spinels yet. However, there is ample evidence for the existence of trigonal distortions in oxide spinels (see, e.g., Refs. [30–32]), rendering there existence in chalcogenide spinels very likely. Since the physical and chemical properties of these compounds strongly depend on the d electrons, it is important to understand the role of electrons on the ionic ordering, lattice distortion, and magnetic properties. Specifically, there are no convincing explanations with respect to the factors that determine the spatial distribution of the cations over the tetrahedral or octahedral sites and also with regard to the dependence of the activation barriers for migration on the doping level.[33,34] Studies on concerted migration[35] and the impact of the structural framework on the ionic conductivity[36] were carried out to analyze the factors determining the energy barriers for migration. However, there are still open questions regarding the cation ordering within the lattice and ion mobility in the various concentrations.

In this paper we report first-principles electronic structure calculations addressing the Mg-ion mobility in MgB_2X_4 spinel structures. We particularly focus on the electronic properties determining ion migration in these materials. We find a strong dependence of the stability of the octahedral vs. the tetrahedral sites on the ion concentration which we explain by an octahedral distortion and the corresponding changes in the lattice constants. Based on

geometric considerations, we identify the ratio of distances in the octahedron and tetrahedron k_{64} as a descriptor for the stability of the cations within the octahedral and tetrahedral sites in the spinel lattice. In addition, we show that a pure ionic interaction picture is insufficient to capture the physics and chemistry behind the ionic migration and site preference. These insights also provide a framework for proposing promising spinel materials with a high ion-mobility based on fundamental materials properties.

Computational details

First-principles calculations have been carried out in the framework of density-functional theory (DFT)[37,38] in order to determine the properties of MgB_2X_4 (B = Sc, Ti, V, Cr, Mn, Fe, Co, Ni, Y, Al and X = S, Se) spinel with regard to Mg migration. Exchange-correlation effects are approximated within the generalized gradient approximation (GGA) using the Perdew-Burke-Ernzerhof (PBE) functional.[39] The calculations are performed employing the Projector Augmented Wave (PAW)[40] method as implemented in the Vienna *Ab-initio* Simulation Package.[41–43] The nudged elastic band (NEB)[44] method is used to determine Mg-ion migration barriers. A 2×2×2 supercell of the primitive spinel cell is constructed for the NEB calculations, including 56 atoms. The total energy has been evaluated with a 2×2×2 k-point mesh. A plane wave cutoff of 520 eV has been chosen in the expansion of the wave functions, and total energies have been converged within 1×10^{-5} eV per supercell.

Mg-ion migration in the chalcogenides has been studied in the low (one Mg vacancy per supercell) and high (one Mg inside supercell) vacancy limit. The structures were fully relaxed until the forces on the atoms were converged within 0.05 eV $Å^{-1}$. The NEB calculations have been carried out with four distinct images between the tetrahedral and octahedral sites to evaluate the Mg-ion migration trajectory. To minimize the interaction between the migrating Mg ions across periodic boundaries, a distance of 10 Å between them has been chosen.

The Mg intercalation energy E_{inter} in the spinel structure with respect to a metallic

magnesium anode is given by

$$E_{inter}(\mathrm{Mg}) = E(\mathrm{Mg_{x+y}B_2X_4}) - (E(\mathrm{Mg_yB_2X_4}) + xE(\mathrm{Mg})) \ , \tag{1}$$

where $E(\mathrm{Mg_yB_2X_4})$ is the total energy of the spinel with a Mg concentration y in the unit cell, and $E(\mathrm{Mg})$ is the cohesive energy of Mg bulk in the metal phase. The corresponding open circuit voltage (V_{OC}) is then given by

$$V_{OC} = -\frac{E_{inter}}{zF}, \tag{2}$$

where F is the Faraday constant and z corresponds to the elementary charges that are transferred upon the discharging reaction with $z = 2$ for Mg-ion batteries. When E_{inter} is expressed in eV, then V_{OC} in volts is simply given by $E_{inter}/2$ for Mg-ion batteries.

Results and Discussion

Among the complex transition-metal (B) oxides and chalcogenides, spinel structure with the composition $\mathrm{Mg^{2+}B_2^{3+}X_4^{2-}}$ correspond to the most promising Mg-ion conductors.[28,45,46] The spinel structure, illustrated in Fig. 1, consists of a face-centered cubic lattice of X anions (X = O, S, Se) with two kinds of interstices between the sites of the fcc lattice: tetrahedral interstices $\mathrm{MgX_4}$ and octahedral interstices $\mathrm{BX_6}$. The $\mathrm{BX_6}$ octahedra form a network of edge-sharing chains while the Mg ions are located in the tetrahedrally vacant spaces of X ions, forming the $\mathrm{MgX_4}$ units. The B sublattice of the spinel structure is known as the pyrochlore lattice with a strong geometrical frustration effects. The Mg sublattice forms a diamond lattice. As far as the electronic structure of the transition metal spinels are concerned, the d-orbitals split into the high-lying doubly degenerate e_g and low-lying triply degenerate t_{2g} orbitals caused by the crystal field splitting of the regular $\mathrm{BX_6}$ octahedron.

Note that it is well-known that spinel oxides tend to exhibit a strong Jahn-Teller distor-

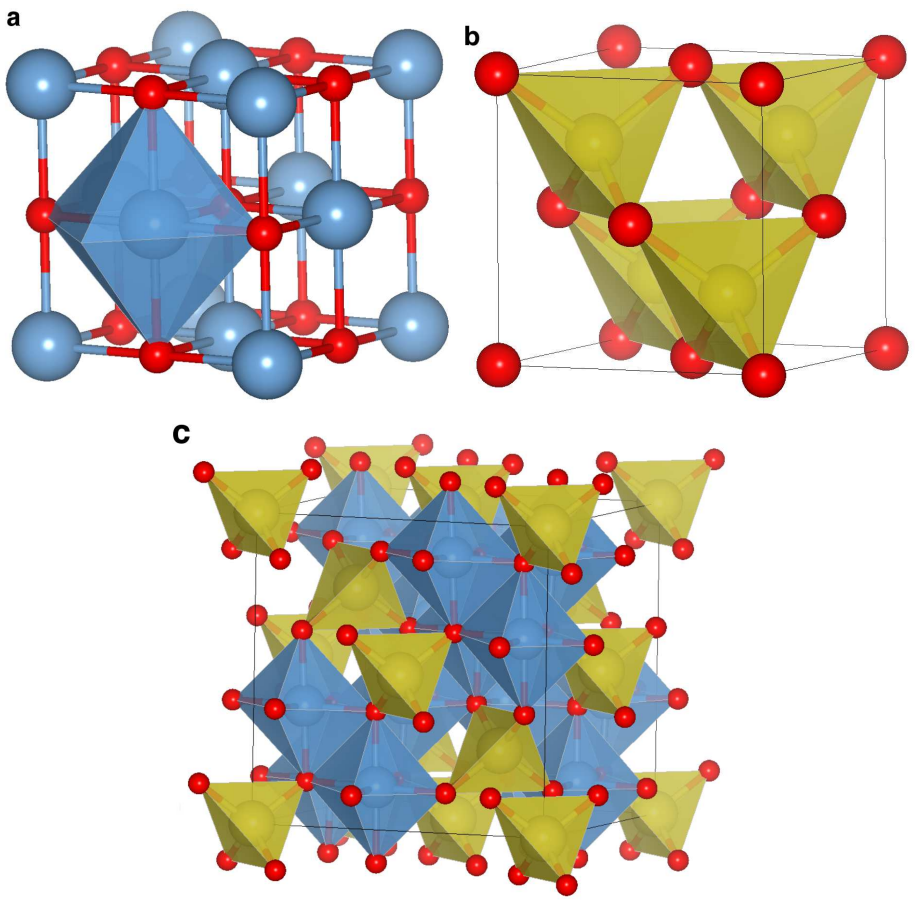

Figure 1: (a) Rock-salt, (b) zinc-blende, and (c) spinel structure. The spinel lattice is an ordered mixture of the zinc-blende and rock-salt structure. The A species (yellow) of AB_2X_4 occupy the tetrahedral sites, while the B species (blue) only occupy octahedral sites. The red spheres denote the oxide and chalcogenide anions such as O^{2-}, S^{2-}, and Se^{2-}.

tion upon lithium insertion which leads to a reduction of the crystal symmetry from cubic to tetragonal symmetry. For example, the lithiation of the $LiMn_2O_4$ spinel to $Li_{2.2}Mn_2O_4$ is accompanied by a tetragonal distortion characterized by a c/a ratio of $c/a = 1.16$.[47,48] On the other hand, increasing the average oxidation state of manganese in these lithium manganospinels from 3.5+ to 4+ causes the suppresses of the Jahn-Teller distortion connected at the same time with a transition from antiferromagnetic to ferromagnetic behavior.[49] In our calculations of the sulfide and selenide spinels, we carefully looked for possible Jahn-Teller distortions, but could not detect any. We attribute this to the predominant ferromagnetic order of these spinels which make them much more conducting than oxides

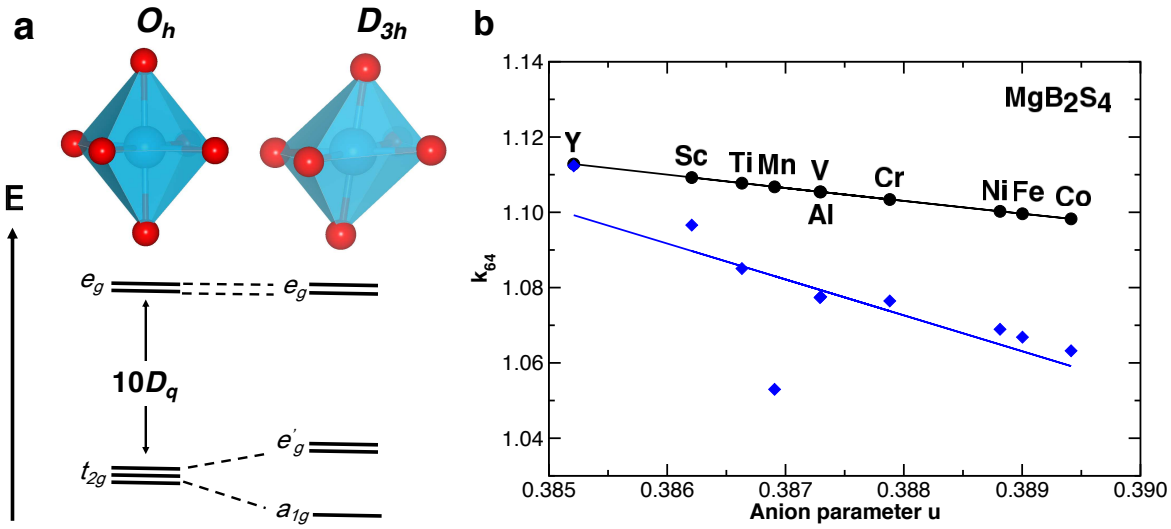

Figure 2: (a) Illustration of the transition from an undistorted octahedron cage with a O_h octahedral symmetry to a trigonally distorted cage with a D_{3h} octahedral symmetry and the associated further crystal field splitting of the d-states. (b) Dependence of the ratio k_{64} on the anion parameter u characterizing the trigonal distortion for S-spinels. The black dots denote the results for the original spinel structures with the Mg ion in a tetrahedral site and the octahedral vacancy being empty, and the black line corresponds to the analytical expression Eq. 5. The blue diamonds are determined for the relaxed spinels with the octahedral site occupied by a Mg anion. The blue line is a linear regression of these results. Note that the results for V and Al lie on top of each other for both considered cases.

due to the enhanced p-d hybridization. Note furthermore that spinel oxides are also prone to spin inversion and that sulfide spinels such as $MgIn_2S_4$ have been shown to exhibit an inverted spinel structure.[50] However, to the best of our knowledge the number of sulfide and selenide spinels with an inverted structure is still limited. For example, it has been carefully verified that $MgSc_2Se_4$ does not exhibit inversion.[25] We also attribute this to the higher conductivity of sulfide and selenide spinels associated with more delocalized electronic states which suppresses high-spin states and thus strong ligand-field stabilization which would favor spinel inversion.

However, spinel structures often exhibit a trigonal distortion of the octahedra that corresponds to a displacement of the X-ions along the [111] direction and changes the O_h octahedral symmetry to a D_{3h} octahedral symmetry but keeps the overall octahedral shape unchanged (see Fig. 2a).[51] The trigonal distortion can be characterized by a u anion param-

eter[52] that reflects the displacement of the X-ions along the [111] direction in units of the lattice constant a. Sickafus et al.[52] showed that this parameter can be expressed through the effective radii $r(\mathrm{Mg})$ and $r(\mathrm{B})$ of the Mg and metal cations, respectively, according to

$$u = 0.3876 \left(\frac{r(\mathrm{B})}{r(\mathrm{Mg})} \right)^{-0.07054} . \tag{3}$$

Interestingly, the effective radius of the X anions does not enter this expression which means that the size of these anions obviously does not affect the trigonal distortions. For a value of $u = \frac{3}{8}$, an ideal spinel structure without any trigonal distortion results. $u > \frac{3}{8}$ is associated with a trigonal distortion of the octahedra through which the tetrahedrons are enlarged at the expense of the octahedrons whereas it is the other way around for $u < \frac{3}{8}$. The trigonal distortion of the octahedron further divides the threefold degenerate t_{2g} states into a lower a_{1g} state and a twofold degenerate e'_g states as illustrated in Fig. 2a. It should be noted that the representation of the a_{1g} state is $\frac{1}{\sqrt{3}}(xy + yz + zx)$, pointing towards the center of the B-lattice tetrahedron. The e'_g states are different from the doubly degenerate e_g states and they are perpendicular to the a_{1g} state. At low temperatures,[53] alternatively a tetragonal distortion often occurs which splits the threefold degenerate t_{2g} states into a higher xy state and the twofold degenerate yz/zx lower states. The tetragonal distortion divides the doubly degenerate e_g states as well into $x^2 - y^2$ and $3z^2 - r^2$ states. Note, however, that the splitting of the t_{2g} states illustrated in Fig. 2a is exaggerated, the calculated splitting is much smaller. Therefore we will in the following still refer to these two groups of states by calling them e_g and t_{2g} states for the sake of convenience.

Besides the additional cystal field splitting, the trigonal distortions also modify the bonding distances, as mentioned in the previous paragraph. This can be quantified by explicitly looking at the Mg-X distances $d(cn_4)$ and $d(cn_6)$ in the tetrahedral and octahedral sites, respectively. In the original spinel structures with the Mg ion in a tetrahedral site and the octahedral vacancy being empty, these distances can be expressed as a function of the anion

parameter u as,[52]

$$\begin{aligned} d(cn_4) &= (u - \frac{1}{4})a\sqrt{3} \ , \\ d(cn_6) &= \left(2(u - \frac{3}{8})^2 + (u - \frac{1}{8})^2\right)^{1/2} a \ . \end{aligned} \tag{4}$$

Using Eq. 4, the ratio k_{64} between the bond lengths in the octahedral and the tetrahedral sites is given by

$$k_{64} = \frac{d(cn_6)}{d(cn_4)} = \frac{\left(2(u - \frac{3}{8})^2 + (u - \frac{1}{8})^2\right)^{1/2} a}{(u - \frac{1}{4})a\sqrt{3}} \overset{u=0.375}{=} \frac{2}{\sqrt{3}} \ . \tag{5}$$

Here we indicated that in the perfect crystal with $u = 3/8 = 0.375$ the ratio is $k_{64} = 2/\sqrt{3} \approx 1.15$ which means that in this structure the Mg-X bond length in the octahedral sites is 1.15 times larger than the tetrahedral bond length.

In Fig. 2b, we have plotted the ratio k_{64} as a function of the anion parameter u for a number of ternary Mg spinels. The upper black circles correspond to the values for the Mg ion in a tetrahedral site and the octahedral vacancy being empty. It is obvious that k_{64} decreases approximately linearly with u in the small considered interval of u values which are larger than the value of 0.375 for the ideal structure, i.e., for all considered spinels the size of the tetrahedra is enlarged at the expense of the octahedron.

Furthermore, it is important to note that in the presence of the Mg ions in the octahedral vacancy, k_{64} is further reduced as illustrated by the blue symbols in Fig. 2b. Hence due to the explicit interaction of Mg cations with the surrounding chalcogenide anions, the size of the octahedrons further shrinks with respect to the tetrahedron. The dependence of k_{64} on u is in general still linear, but there are outliers. This is particularly obvious for $MgMn_2S_4$ where the presence of Mn apparently leads to a significant compression of the occupied octahedron. Interestingly enough, the size of the trigonal distortions is not exactly ordered according to d-state occupation but rather according to decreasing crystal ionic radii as listed by Shannon,[54] suggesting that the change in these radii acts as one of the main driving forces

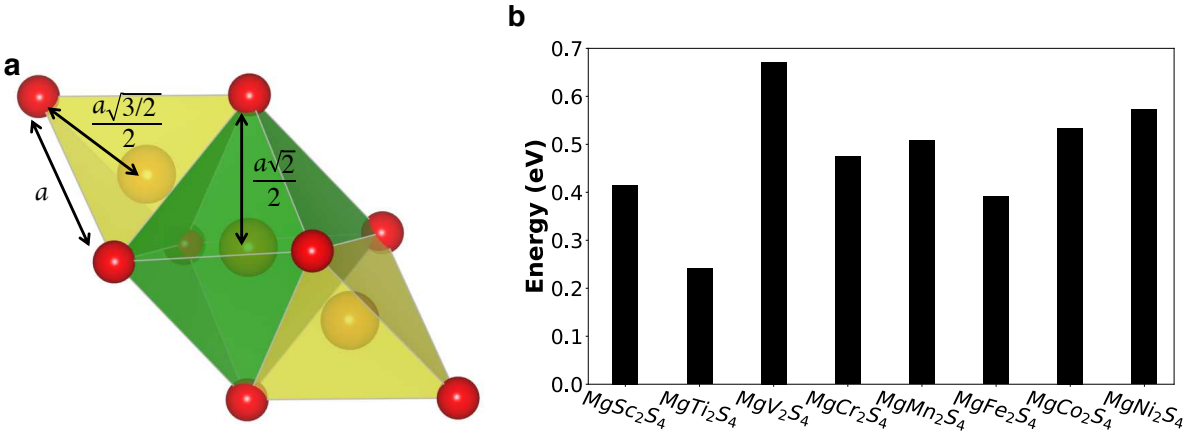

Figure 3: (a) Illustration of single-ion migration from tetrahedral site to the octahedral void and then to the next tetrahedral site. The chalcogenide atoms such as S and Se are shown by the red spheres, the migrating Mg ion is presented by the spheres inside the tetrahedrons and the octahedron. (b) Calculated Mg migration barriers for several transition metal ions in the sulfide-spinels.

for the trigonal distortions.

We now focus on the Mg mobility in the ternary spinel structures. The Mg-ion migration occurs between two tetrahedral sites via the migration across the face-sharing octahedral void which is shown in Fig. 3a. The transition state for the Mg migration is located in the triangular face between the octahedral and tetrahedral sites. The magnitude of the activation energy E_a is influenced by the anion species and the size of the triangle. Oxide cathode materials typically exhibit sluggish Mg^{2+} migration kinetics and also limited cycle lifes. The magnitude of the Mg^{2+} migration barriers can be reduced by introducing a soft anion (i.e. S, Se, Te) lattice.[25,55,56] This leads to a weaker Coulombic attraction and a larger lattice constant which also increases the distance between the guest Mg^{2+} and the host lattice, thus enhancing ion mobility. However, an increase in the ion mobility is typically associated with a reduction of energy density because low diffusion barriers are usually accompanied by small intercalation energies.

Fig. 3b shows the calculated Mg^{2+} migration barriers of some selected sulfide spinels. All compounds represent Mg-ion migration energy smaller than 0.7 eV, confirming the relatively good Mg^{2+} conductivity in these spinel structures. $MgTi_2S_4$ is identified as a suitable Mg-ion

conductor, however, this compound is found to be unstable in the spinel structure and to exhibit electronic conductivity.[57] Sulfide spinels enhance the p-d hybridization compared to oxides and tend to be more conducting. The various transition metal ions with d^1 up to the d^{10} configurations lead to magnetic structures that are caused by the strong Coulomb repulsion within the d-orbitals.[58] In addition, smaller crystal ionic radii of the transition metals lead to decreased atomic distances and add more trigonal distortion to the system, as shown in Fig. 2b. This obviously increases the Mg migration barriers. Hence transition metals with occupied d-orbitals in general reduce the Mg-ion conductivity depending on the particular orbital character. Transition metal ions such as Sc with empty d-orbitals, on the other hand, lead to small migration barriers. In particular, the $MgSc_2S_4$ spinel compound represents a balance between small Mg^{2+} migration energies and sufficient structural stability. Thus, in the following we will only focus on MgB_2X_4 compounds with empty d-orbitals which are characterized by a high Mg-ion mobility according to our calculations. It is interesting to note that an analogous trend has been found in a recent computational study of Mg migration in lanthanoid chalcogenide spinels.[29] In these systems, apparently the height of the Mg migration barriers increases with higher f-state occupancy.

In order to elucidate the influence of the electronic structure on the properties of the spinels, we have plotted in Fig. 4 the density of states (DOS) of MgB_2X_4 spinels with B =Sc and Y, and X = S and Se that can be realized experimentally.[59,60] Note that these spinel structures also exhibit trigonal distortions, but they are smaller than those for the spinels with later d-band metals, as shown in Fig. 2b. In Sc and Y, the d-orbitals are empty which leads to unoccupied t_{2g} (green) and e_g (yellow) manifolds. In both compounds with Sc and Y cations, respectively, the valence bands are dominated by S- and Se-p bands, respectively, in the energy range from $-4\,\mathrm{eV}$ to $0\,\mathrm{eV}$. For both systems, the DOS of the t_{2g} and e_g states is rather broad and overlaps with each other. The main effect of replacing S ions by Se ions is a reduction of the band gap by about 0.5 eV and a smaller ligand field splitting between anti-bonding e_g and non-bonding t_{2g} states. In the valence band depicted in Fig. 4, d-derived

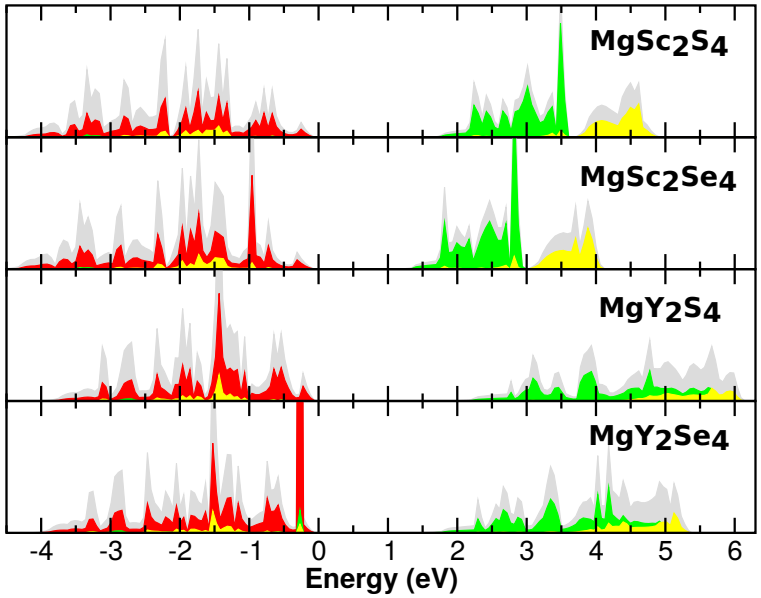

Figure 4: Density of states for $MgSc_2S_4$, $MgSc_2Se_4$, MgY_2S_4, and MgY_2Se_4 from top to bottom. The total DOS is given in gray. The projected DOS are shown in red for S and Se, in green for t_{2g} and yellow for e_g d-orbitals. The energy zero is set to the top of the valence band.

states appear although Y and Sc in principle have no occupied d-states in the conduction band. These states originate from the hybridization between the d-states of the transition metal and the chalcogenides p bands,[61] but they do not dominate the behavior of the valence band.

Due to the absence of d valence states in Sc and Y, these elements are not easy to oxidize or to reduce upon intercalation. Hence the chalcogenide anions need to be involved in the associated redox processes. In fact, this anion-based redox chemistry (anionic redox) has recently drawn quite some attention with respect to the increase in the energy density of Li-, Na- and Mg-ion batteries, see, e.g., Refs.[62,63] To elucidate this anionic redox, we performed a Bader charge analysis[64] and calculated charge density differences[65] for $MgSc_2S_4$. Details of this charge analysis can be found in the Supplementary Information. Specifically, we considered the insertion of Mg into an octahedral site of the host Sc_2S_4 lattice at a low concentration resulting in a $Mg_{0.125}Sc_2S_4$ structure. We find that this insertion leads to a reduction of the sulfur atoms reflected by a change of the S Bader charge from $-0.86\,e$ to

$-1.08\,e$ (see Fig. S2), whereas Sc hardly participates in the reduction process. This confirms previous findings that the classical description of the redox process is no longer valid when the Fermi level becomes close to the S/Se-p band.[62]

In fact, even for spinel transition metals containing a finite number of d electrons anionic redox can occur, as our calculations for $MgCr_2S_4$ show. Upon Mg insertion into the Cr_2S_4 host lattice at a high Mg concentration, the S atoms become reduced from a Bader charge of $-1.02\,e$ to $-1.30\,e$, which is much stronger than the accompanying reduction of the Cr atoms. In contrast, in $MgCr_2O_4$ both the Cr-d and O-p orbitals participate in a comparable fashion in the redox process according to our calculations (see Supporting Information). This indicates that in sulfide and selenide spinels the anionic redox should be much more dominant than in oxide spinels which can be traced back to the much lower electronegativity of the chalcogenides S and Se compared to oxygen.

Table 1 lists calculated properties of the considered spinel systems. These include structural properties of $Mg(Sc/Y)_2(S/Se)_4$ spinels, the Mg migration barrier, the Mg intercalation energy and the open-circuit voltage in the high and low Mg concentration limit, and the volume change upon Mg intercalation. Based on the calculations, MgY_2Se_4 is a favorable candidate due to the combination of a small migration barrier, an sufficiently large open-circuit voltage, and a small volume change. $MgSc_2Se_4$ and MgY_2S_4 are also characterized by parameters which make them suitable as Mg-ion conductors. However, the performance of

Table 1: Mg-X, B-X, B-B, and Mg-Mg bond lengths in Å for spinel compounds. B and X denote transition-metal (Sc, Y) and anion (S, Se) respectively. Calculated relative barrier energy E_a, intercalation energy E_{inter}^{high} (E_{inter}^{low}) (Eq. 1) for high (low) Mg concentration in eV, and corresponding open-circuit voltage V_{OC}^{high} (V_{OC}^{low}) in V. The volume changes with respect to the structure without Mg is indicated by $\Delta V/V$.

Compound	Mg-X (Å)	B-X (Å)	B-B (Å)	Mg-Mg (Å)	E_a(eV)	E_{inter}^{high} (eV)	V_{OC}^{high} (V)	E_{inter}^{low} (eV)	V_{OC}^{low} (V)	$\Delta V/V$ (%)
$MgSc_2S_4$	2.464	2.593	3.784	4.634	0.415	-5.149	2.574	-5.165	2.582	-10
$MgSc_2Se_4$	2.587	2.725	3.974	4.868	0.375	-3.915	1.958	-4.114	2.057	-5
MgY_2S_4	2.510	2.740	3.949	4.836	0.360	-5.508	2.754	-5.561	2.780	+4.8
MgY_2Se_4	2.624	2.868	4.131	5.059	0.361	-4.329	2.165	-4.432	2.216	-2

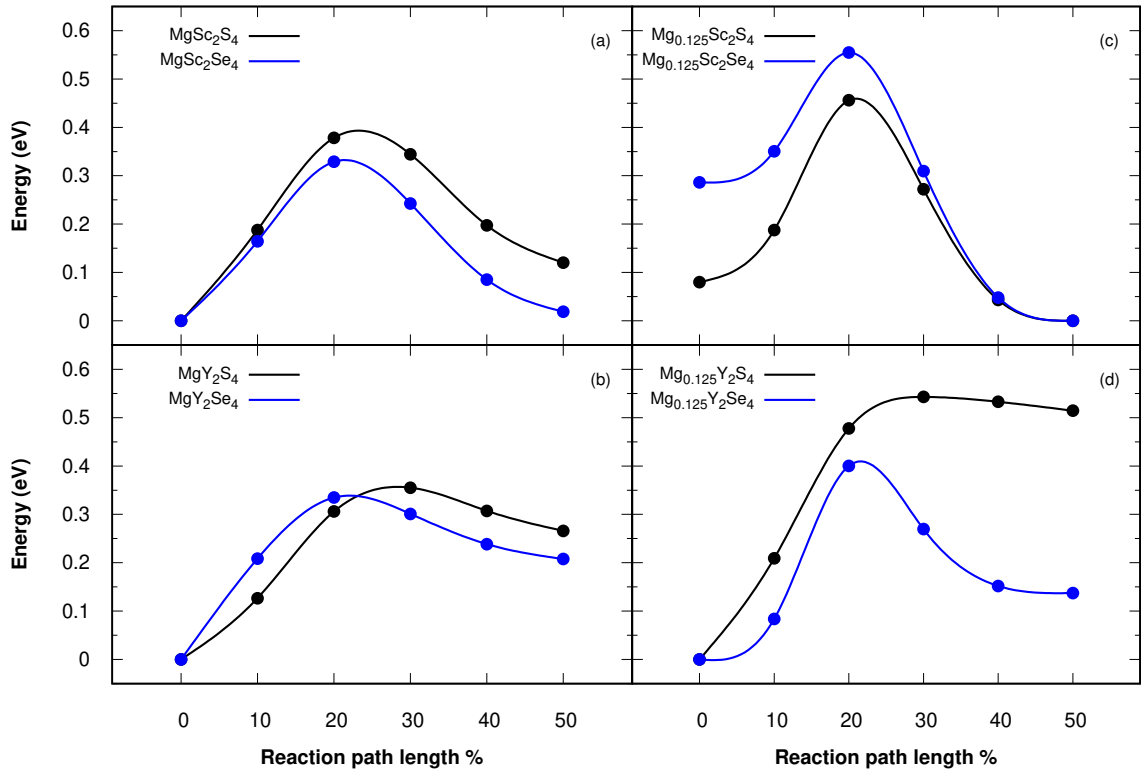

Figure 5: The Mg^{2+} migration energy barriers (in eV) as a function of the reaction path coordinate derived from periodic DFT calculations combined with NEB for the single-ion migration from tetrahedral site to the octahedral void corresponding to the S-spinels (black) and the Se-spinels (blue) for low and high concentrations of Mg ions. Note that the full migration path in principle includes the further migration from the octahedral to the tetrahedral site, but as the corresponding energies are symmetric with respect to the octahedral site, this part is omitted.

MgY_2S_4 is detoriated, in spite of a high open-circuit voltage V_{OC}, by an unfavorable volume expansion of almost 5% after Mg-ion removal.

In order to further assess the ion mobility in these spinels structures, the energies along the Mg migration paths for $MgSc_2(S/Se)_4$ and $MgY_2(S/Se)_4$ in the high and low concentration of Mg-ion are plotted in Fig. 5. Note that in the high Mg-ion concentration limit, there are 7 Mg ions in the 2×2×2 supercell located in the tetrahedral sites one of which is migrating, whereas in the high Mg-ion concentration limit, there is only one Mg ion in the supercell that is also the migrating ion. The Mg-ion migration barriers of MgY_2S_4 ($\sim$ 360 meV), MgY_2Se_4

($\sim$ 361 meV), and $MgSc_2Se_4$ ($\sim$ 375 meV) in the high Mg concentration limit are rather small leading to a high Mg mobility which is comparable to Li^+ in fast Li-conductors. This suggests that S- and Se-spinel structures together with Sc and Y cations can act as excellent Mg conductors. Furthermore, the band gaps of about 1.5 eV for the selenides and of about 2 eV for the sulfides should lead to a relatively low electron conductivity. Hence in principle, these materials might as well be considered as promising candidates for solid electrolytes in Mg-ion batteries because of their high Mg-ion mobility. However, experiments still found a high electron conductivity in these compounds,[22] probably due to the presence of defects or phase deformations,[25,28] hindering their use as solid electrolytes, but thus making them suitable as electrode materials with a high ion mobility.

In the low Mg concentration limit, the Mg-ion migrations barriers in the S- and Se-spinels are increased compared to the high concentration limit, as shown in Fig. 5. Furthermore, in $Mg_{0.125}Sc_2(S/Se)_4$ the Mg-ion prefers the six-fold coordination of the octahedral site, whereas in $Mg_{0.125}Y_2(S/Se)_4$ the Mg-ion prefers the fourfold coordination of the tetrahedral site. Thus in the S- and Se-spinels structures together with Sc the most favorable site for the Mg-ion changes from the octahedral to the tetrahedral site upon increasing the Mg concentration. This varying site preference, which is not the case for the Y cation, might be detrimental for the performance of the Sc-containing cathodes upon charge/discharge. In addition, the $MgY_2(S/Se)_4$ compounds exhibit smaller relative volume changes upon the addition of Mg atoms than the $MgSc_2(S/Se)_4$ compounds, which might partly due to the fact that Y has a larger crystal ionic radius than Sc.[54]

Up to now, we have concentrated on the electronic properties, structural parameters, and Mg migration paths. Of particular interest is that all $Mg(Sc/Y)_2(S/Se)_4$ compounds favor the tetrahedral sites for the Mg ions. However, in the low Mg concentration limit, Mg ions prefer the octahedral site in the Sc spinels. In order to analyze this behavior, we will first concentrate on the high Mg concentration limit. Interestingly, according to our calculations Mg^{2+} tends to occupy the octahedral sites in the $MgMn_2S_4$ spinel in the high

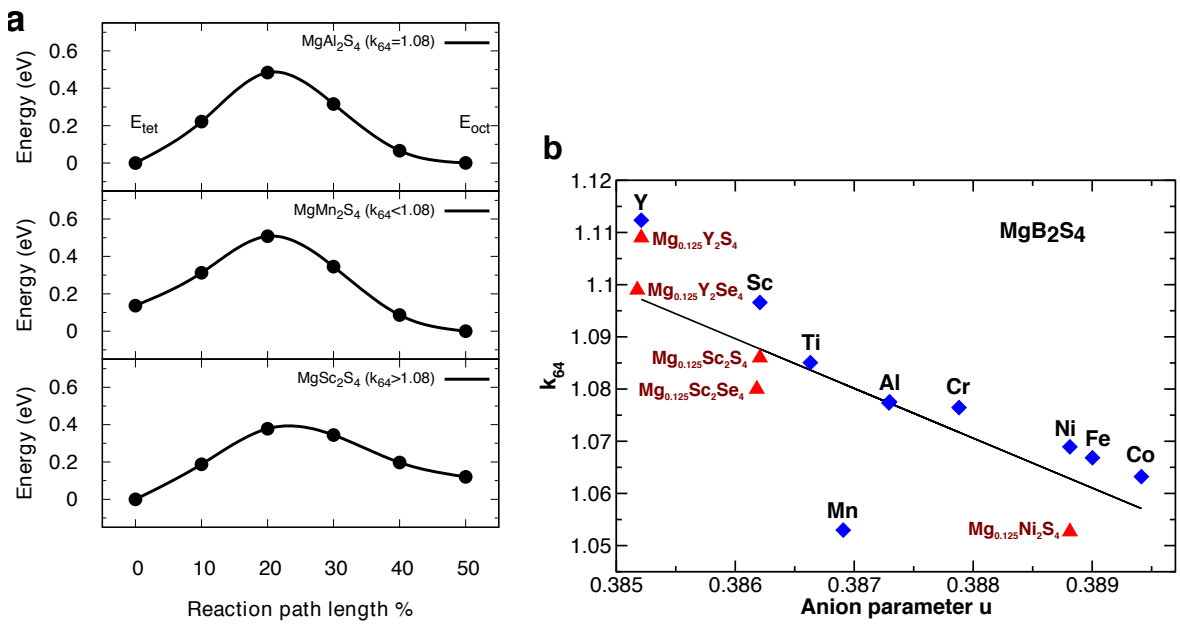

Figure 6: (a) Mg-ion migration barriers for spinel compounds with different trigonal distortions characterized by k_{64}. (b) The ratio k_{64} as a function of the anion parameter u for selected spinel compounds. Blue diamonds denote high Mg concentration compounds and red triangles low Mg concentration compounds. The black line represents a dividing line between Mg tetrahedral and octahedral site preference.

Mg concentration limit. Here we will show that it is the competition between coordination and bond length induced by the trigonal distortion that governs the Mg site preference in ternary spinel compounds MgB_2X_4 (B = Sc, Ti, V, Cr, Mn, Fe, Co, Ni, Y, Al and X = S, Se).

In order to see this, we focus on the ratio k_{64} between the Mg-X bond length in the occupied tetrahedral and octahedral sites, as shown for some ternary spinels by the blue symbols in Fig. 2b. According to our calculations, for the $MgAl_2S_4$ system characterized by a ratio of about $k_{64} = 1.08$, the octahedral and the tetrahedral site become energetically degenerate with regard to the Mg occupation, as illustrated in Fig. 6a. This can be explained by a competition between bond length and coordination as a function of the ratio k_{64}. The octahedral site has the higher coordination than the tetrahedral site, but obviously in the ideal structure the elongation of the Mg-X bond length by 1.15 with respect to the tetrahedral sites makes the octahedral site energetically still less favorable. However, for decreasing ratio

k_{64} the octahedral site becomes increasingly more stable with respect to the tetrahedral site. Note that the ratio $k_{64} = 1.08$ is still larger than 1, but at this value the larger bond length is compensated by the higher coordination of the octahedral site. For even smaller values of k_{64}, as for example in $MgMn_2S_4$ with $k_{64} = 1.05$, the octahedral site is energetically more favorable whereas for larger values of k_{64} as in $MgSc_2S_4$ with $k_{64} = 1.10$, the tetrahedral site becomes preferred (see Fig. 6a).

A similar reasoning has recently been presented in order to understand the Mg tetrahedral site preference in lanthanoid chalcogenide spinels,[29] based on the concept that the preference for coordination of a cation by an anion can be estimated by classic radii ratio rules. This argumentation about the competition between bond length and coordination implicitly assumes that the interaction is purely ionic between non-polarizable atomic charges so that the ionic interaction is additive. Let us make a simple estimate about the stability of the tetrahedral Mg-X_4 site vs. the octahedral Mg-X_6 site assuming that only the direct interaction between the Mg^{2+} cation and the neighbouring chalgonide X^{2-} anions contribute to the interaction. For non-polarizable, sperically symmetric and non-overlapping charges, the binding energies E(Mg-X_4) and E(Mg-X_6) in the tetrahedral and the octahedral arrangement, respectively, are given by

$$\begin{aligned} E(\mathrm{Mg-X_4}) &= 4\frac{Q_{\mathrm{Mg^{2+}}}Q_{\mathrm{X^{2-}}}}{d(cn_4)} = -\frac{16}{d(cn_4)}, \\ E(\mathrm{Mg-X_6}) &= 6\frac{Q_{\mathrm{Mg^{2+}}}Q_{\mathrm{X^{2-}}}}{d(cn_6)} = -\frac{24}{d(cn_6)}, \end{aligned} \tag{6}$$

where we have used cgs units for the sake of simplicity. For this purely ionic interaction the binding energies are the same, i.e., E(Mg-X_4) = E(Mg-X_6), for a ratio of

$$k_{64}^{\text{ionic eq.}} = \frac{d(cn_6)}{d(cn_4)} = 1.5 \ . \tag{7}$$

First of all note that this ratio of 1.5 is much larger than the value of $k_{64} = 1.08$ at which there is an equilbrium between tetrahedral site and octahedral site in $MgAl_2S_4$. In addition,

the fact whether a spinel exhibits a tetrahedral or an octahedral site preference does not only depend on the ratio k_{64}, but also on the anion parameter u. In Fig. 6b, we again show the ratio k_{64} as a function of the anion parameter u, but now we also include some additional data points for the low Mg-concentration limit. In addition, we have inserted a dividing line given by $k_{64}^{div} = 4.78(1-2u)$. In spinels above this line, the migrating Mg ions prefer the tetrahedral site whereas in those below this line, the octahedral site is more stable. Thus for larger values of u, the octahedral become more stable than the tetrahedral sites only for smaller values of the ratio k_{64}. On the other hand, in the compounds nearby the dividing line, such as Ti, the occupation of both the tetrahedral and octahedral sites is energetically feasible, as also confirmed experimentally.[24]

In order to understand this trend, one should first note that according to Eq. 4 both distances $d(cn_4)$ and $d(cn_6)$ become larger with increasing u in the parameter range that is considered here. However, for purely ionic interactions between non-polarizable spherically symmetric ions, the competition in the energetic stability between two different structures does not depend on the absolute distances, only on the ratio of distances,[29,66–68] as reflected in the simple estimate Eq. 7. Consequently, these results can only be explained assuming that the interaction is not purely ionic and that it falls off stronger than $1/d$ with distance d. Or, in other words, *covalent interactions contribute substantially to the stability of the Mg atoms in the voids*. Hence it follows that there is a simple criterion or descriptor that allows to identify whether covalent interactions play a critical role in the relative stability of different structures: If the relative stability does not only depend on the ratio of distances but also on the absolute value of these distances, then the interaction in these systems cannot be purely ionic.

The important role of covalent contributions in the interaction within the spinels is also reflected in the significant width in the density of states of the chalgonide-derived states shown in Fig. 4. For covalent and metallic interactions, the strengths of single bonds typically decreases with increasing coordination[15] based on bond-order conservation arguments,

so that the single bond becomes weaker for higher coordination. Furthermore, these interactions scale with the overlap between atomic orbitals which falls off exponentially for larger distances. Hence, the ratio $k_{64} = d(cn_6)/d(cn_4)$ needs to become smaller for absolute larger distances, i.e., for larger values of u, to make the octahedral more stable than the tetrahedral site.

Our findings provide a simple picture of the key parameter underlying Mg-ion site preferences in spinel structures. Similar to the Goldschmidt tolerance factor t[66] which is used to reflect the variance in the stability of perovskites based only on the ratio of the atomic radii of A, B, and X in ABX_3, we use a geometrical analysis to assess the relative stability of the Mg^{2+} sites in spinels. Our calculations and considerations of the structure of the spinel compounds clearly indicate that it is the ratio *together* with the absolute values of the Mg-X bond lengths in the octahedral and tetrahedral sites that determines the site preference and thus also the Mg mobility.

Conclusions and Summary

Based on periodic density functional theory calculations, we have studied Mg ion mobility in spinel chalcogenides which are promising candidates for cathodes in Mg-ion batteries. Overall, we find that trigonal distortions of the spinel structures play a critical role for both the Mg site preference as well as for the Mg migration barriers. With respect to the transition metal used in the spinels we find that an increasing d-band occupancy leads to smaller lattice constants and larger trigonal distortions which both lead to larger migration barriers and thus decreasing diffusitivities. In addition, according to our calculations anionic redox upon Mg insertion into the host lattice is more dominant in sulfide and selenide spinels than in oxide spinels. Hence we concentrated on spinel chalcogenide compounds with the early d-band metals Sc and Y together with the soft ion chalcogenide S and Se.

Indeed, all these four considered spinels exhibit small diffusion barriers of about 400

meV and smaller. In addition, these materials allow open-circuit potentials with respect to metallic Mg of about 2.5 V for the sulfides and of about 2.0 V for the selenides. This makes them theoretically well-suited as cathode materials for Mg-ion batteries. On the other hand, the low diffusion barriers together with the band gap of about 1.5 eV for the selenides and of about 2 eV for the sulfides limiting their electronic conductivity suggests that these materials could also be used as solid electrolytes in Mg-ion batteries because of their high Mg-ion mobility.

In many spinel structures studied so far, the tetrahedral sites exhibits a higher stability than the octrahedral sites for Mg insertion. Interestingly, we find that in the Sc-based spinels this stability is reversed in the low Mg concentration limit. Our detailed analysis reveals that the varying site preference is a consequence of the competition between coordination and bond length induced by trigonal distortions and absolute changes in the bond distances demonstrating the important role of covalent contributions to the chemical interaction within the spinels. Thus considering only purely electrostatic interactions is inadequate for capturing all factors influencing ion mobility and stability. In general, our results and the analysis based on electronic and geometric factors provide a conceptual framework to understand fast ion conductivity in spinel electrode materials that will also be beneficial for the understanding and improvement of ion mobility in other materials classes.

Acknowledgements

M.S. thanks Sung Sakong and Mohnish Pandey for fruitful discussions. Financial support from the Cluster of Excellence POLiS (EXC-2154, project ID 390874152) of the Deutsche Forschungsgemeinschaft (DFG) and computer time provided by the state of Baden-Württemberg through bwHPC and the German Research Foundation (DFG) through grant no INST 40/575-1 FUGG (JUSTUS 2 cluster) are gratefully acknowledged.This work contributes to the research performed at CELEST (Center for Electrochemical Energy Storage Ulm-

Karlsruhe).

References

[1] Muldoon, J.; Bucur, C. B.; Gregory, T. Quest for Nonaqueous Multivalent Secondary Batteries: Magnesium and Beyond. *Chem. Rev.* **2014**, *114*, 11683–11720.

[2] Canepa, P.; Sai Gautam, G.; Hannah, D. C.; Malik, R.; Liu, M.; Gallagher, K. G.; Persson, K. A.; Ceder, G. Odyssey of Multivalent Cathode Materials: Open Questions and Future Challenges. *Chem. Rev.* **2017**, *117*, 4287–4341.

[3] Elia, G. A.; Marquardt, K.; Hoeppner, K.; Fantini, S.; Lin, R.; Knipping, E.; Peters, W.; Drillet, J.-F.; Passerini, S.; Hahn, R. An Overview and Future Perspectives of Aluminum Batteries. *Adv. Mater.* **2016**, *28*, 7564–7579.

[4] Anji Reddy, M.; Helen, M.; Groß, A.; Fichtner, M.; Euchner, H. Insight into Sodium Insertion and the Storage Mechanism in Hard Carbon. *ACS Energy Lett.* **2018**, *3*, 2851–2857.

[5] Gregory, T. D.; Hoffman, R. J.; Winterton, R. C. Nonaqueous Electrochemistry of Magnesium: Applications to Energy Storage. *J. Electrochem. Soc.* **1990**, *137*, 775–780.

[6] Aurbach, D.; Lu, Z.; Schechter, A.; Gofer, Y.; Gizbar, H.; Turgeman, R.; Cohen, Y.; Moshkovich, M.; Levi, E. Prototype systems for rechargeable magnesium batteries. *Nature* **2000**, *407*, 724–727.

[7] MacLaughlin, C. M. Status and Outlook for Magnesium Battery Technologies: A Conversation with Stan Whittingham and Sarbajit Banerjee. *ACS Energy Lett.* **2019**, *4*, 572–575.

[8] Davidson, R.; Verma, A.; Santos, D.; Hao, F.; Fincher, C. D.; Zhao, D.; Attari, V.; Schofield, P.; Van Buskirk, J.; Fraticelli-Cartagena, A. et al. Mapping mechanisms and

growth regimes of magnesium electrodeposition at high current densities. *Mater. Horiz.* **2020**, *7*, 843–854.

[9] Singh, N.; Arthur, T. S.; Ling, C.; Matsui, M.; Mizuno, F. A high energy-density tin anode for rechargeable magnesium-ion batteries. *Chem. Commun.* **2013**, *49*, 149–151.

[10] Zhao-Karger, Z.; Gil Bardaji, M. E.; Fuhr, O.; Fichtner, M. A new class of non-corrosive, highly efficient electrolytes for rechargeable magnesium batteries. *J. Mater. Chem. A* **2017**, *5*, 10815–10820.

[11] Aurbach, D.; Cohen, Y.; Moshkovich, M. The Study of Reversible Magnesium Deposition by In Situ Scanning Tunneling Microscopy. *Electrochem. Solid-State Lett.* **2001**, *4*, A113.

[12] Matsui, M. Study on electrochemically deposited Mg metal. *J. Power Sources* **2011**, *196*, 7048 – 7055.

[13] Zhao, Q. S.; Wang, J. L. Reversibility of electrochemical magnesium deposition from tetrahydrofuran solutions containing pyrrolidinyl magnesium halide. *Electrochim. Acta* **2011**, *56*, 6530.

[14] Jäckle, M.; Groß, A. Microscopic properties of lithium, sodium, and magnesium battery anode materials related to possible dendrite growth. *J. Chem. Phys.* **2014**, *141*, 174710.

[15] Jäckle, M.; Helmbrecht, K.; Smits, M.; Stottmeister, D.; Groß, A. Self-diffusion barriers: possible descriptors for dendrite growth in batteries? *Energy Environ. Sci.* **2018**, *11*, 3400–3407.

[16] Levi, E.; Gofer, Y.; Aurbach, D. On the Way to Rechargeable Mg Batteries: The Challenge of New Cathode Materials. *Chem. Mater.* **2010**, *22*, 860–868.

[17] Zhao-Karger, Z.; Liu, R.; Dai, W.; Li, Z.; Diemant, T.; Vinayan, B. P.; Bonatto Minella, C.; Yu, X.; Manthiram, A.; Behm, R. J. et al. Toward Highly Reversible

Magnesium–Sulfur Batteries with Efficient and Practical Mg[B(hfip)4]2 Electrolyte. *ACS Energy Lett.* **2018**, *3*, 2005–2013.

[18] Huie, M. M.; Bock, D. C.; Takeuchi, E. S.; Marschilok, A. C.; Takeuchi, K. J. Cathode materials for magnesium and magnesium-ion based batteries. *Coord. Chem. Rev.* **2015**, *287*, 15 – 27.

[19] Walter, M.; Kravchyk, K. V.; Ibáñez, M.; Kovalenko, M. V. Efficient and Inexpensive Sodium–Magnesium Hybrid Battery. *Chem. Mater.* **2015**, *27*, 7452–7458.

[20] Bucur, C. B.; Gregory, T.; Oliver, A. G.; Muldoon, J. Confession of a Magnesium Battery. *J. Phys. Chem. Lett.* **2015**, *6*, 3578–3591.

[21] Bitenc, J.; Pirnat, K.; Bančič, T.; Gaberšček, M.; Genorio, B.; Randon-Vitanova, A.; Dominko, R. Anthraquinone-Based Polymer as Cathode in Rechargeable Magnesium Batteries. *ChemSusChem* **2015**, *8*, 4128–4132.

[22] Wang, L.-P.; Zhao-Karger, Z.; Klein, F.; Chable, J.; Braun, T.; Schür, A. R.; Wang, C.-R.; Guo, Y.-G.; Fichtner, M. MgSc2Se4—A Magnesium Solid Ionic Conductor for All-Solid-State Mg Batteries? *ChemSusChem* **2019**, *12*, 2286–2293.

[23] Chen, T.; Ceder, G.; Sai Gautam, G.; Canepa, P. Evaluation of Mg Compounds as Coating Materials in Mg Batteries. *Front. Chem.* **2019**, *7*, 24.

[24] Sun, X.; Bonnick, P.; Duffort, V.; Liu, M.; Rong, Z.; Persson, K. A.; Ceder, G.; Nazar, L. F. A high capacity thiospinel cathode for Mg batteries. *Energy Environ. Sci.* **2016**, *9*, 2273–2277.

[25] Canepa, P.; Bo, S.-H.; Sai Gautam, G.; Key, B.; Richards, W. D.; Shi, T.; Tian, Y.; Wang, Y.; Li, J.; Ceder, G. High magnesium mobility in ternary spinel chalcogenides. *Nat. Commun.* **2017**, *8*, 1759.

[26] Islam, M. S.; Fisher, C. A. J. Lithium and sodium battery cathode materials: computational insights into voltage, diffusion and nanostructural properties. *Chem. Soc. Rev.* **2014**, *43*, 185–204.

[27] Groß, A. Fundamental Challenges for Modeling Electrochemical Energy Storage Systems at the Atomic Scale. *Top. Curr. Chem.* **2018**, *376*, 17.

[28] Canepa, P.; Sai Gautam, G.; Broberg, D.; Bo, S.-H.; Ceder, G. Role of Point Defects in Spinel Mg Chalcogenide Conductors. *Chem. Mater.* **2017**, *29*, 9657–9667.

[29] Koettgen, J.; Bartel, C. J.; Ceder, G. Computational investigation of chalcogenide spinel conductors for all-solid-state Mg batteries. *Chem. Commun.* **2020**, *56*, 1952–1955.

[30] Wheeler, E. M.; Lake, B.; Islam, A. T. M. N.; Reehuis, M.; Steffens, P.; Guidi, T.; Hill, A. H. Spin and orbital order in the vanadium spinel MgV_2O_4. *Phys. Rev. B* **2010**, *82*, 140406.

[31] Matsuura, K.; Sagayama, H.; Nii, Y.; Khanh, N. D.; Abe, N.; Arima, T. X-ray magnetic circular dichroism study of an orbital ordered state in the spinel-type vanadium oxide AV_2O_4 ($A = \mathrm{Mn}, \mathrm{Fe}$). *Phys. Rev. B* **2015**, *92*, 035133.

[32] Menon, S. G.; Hebbar, D. N.; Kulkarni, S. D.; Choudhari, K.; Santhosh, C. Facile synthesis and luminescence studies of nanocrystalline red emitting $Cr:ZnAl_2O_4$ phosphor. *Mater. Res. Bull.* **2017**, *86*, 63 – 71.

[33] Goodenough, J. B.; Loeb, A. L. Theory of Ionic Ordering, Crystal Distortion, and Magnetic Exchange Due to Covalent Forces in Spinels. *Phys. Rev.* **1955**, *98*, 391–408.

[34] Goodenough, J. B. Energy storage materials: A perspective. *Energy Storage Mater.* **2015**, *1*, 158 – 161.

[35] He, X.; Zhu, Y.; Mo, Y. Origin of fast ion diffusion in super-ionic conductors. *Nat. Commun.* **2017**, *8*, 15893.

[36] Wang, Y.; Richards, W. D.; Ong, S. P.; Miara, L. J.; Kim, J. C.; Mo, Y.; Ceder, G. Design principles for solid-state lithium superionic conductors. *Nat. Mater.* **2015**, *14*, 1026.

[37] Hohenberg, P.; Kohn, W. Inhomogeneous Electron Gas. *Phys. Rev.* **1964**, *136*, B864–B871.

[38] Kohn, W.; Sham, L. J. Self-Consistent Equations Including Exchange and Correlation Effects. *Phys. Rev.* **1965**, *140*, A1133–A1138.

[39] Perdew, J. P.; Burke, K.; Ernzerhof, M. Generalized Gradient Approximation Made Simple. *Phys. Rev. Lett.* **1996**, *77*, 3865–3868.

[40] Blöchl, P. E. Projector augmented-wave method. *Phys. Rev. B* **1994**, *50*, 17953–17979.

[41] Kresse, G.; Hafner, J. Ab initio molecular dynamics for liquid metals. *Phys. Rev. B* **1993**, *47*, 558–561.

[42] Kresse, G.; Furthmüller, J. Efficient iterative schemes for ab initio total-energy calculations using a plane-wave basis set. *Phys. Rev. B* **1996**, *54*, 11169–11186.

[43] Kresse, G.; Joubert, D. From ultrasoft pseudopotentials to the projector augmented-wave method. *Phys. Rev. B* **1999**, *59*, 1758–1775.

[44] Sheppard, D.; Terrell, R.; Henkelman, G. Optimization methods for finding minimum energy paths. *J. Chem. Phys.* **2008**, *128*, 134106.

[45] Kim, C.; Phillips, P. J.; Key, B.; Yi, T.; Nordlund, D.; Yu, Y.-S.; Bayliss, R. D.; Han, S.-D.; He, M.; Zhang, Z. et al. Direct Observation of Reversible Magnesium Ion Intercalation into a Spinel Oxide Host. *Adv. Mater.* **2015**, *27*, 3377–3384.

[46] Yin, J.; Brady, A. B.; Takeuchi, E. S.; Marschilok, A. C.; Takeuchi, K. J. Magnesium-ion battery-relevant electrochemistry of MgMn2O4: crystallite size effects and the notable role of electrolyte water content. *Chem. Commun.* **2017**, *53*, 3665–3668.

[47] Thackeray, M.; David, W.; Bruce, P.; Goodenough, J. Lithium insertion into manganese spinels. *Mater. Res. Bull.* **1983**, *18*, 461 – 472.

[48] Thackeray, M. M.; de Kock, A.; Rossouw, M. H.; Liles, D.; Bittihn, R.; Hoge, D. Spinel Electrodes from the Li-Mn-O System for Rechargeable Lithium Battery Applications. *J. Electrochem. Soc.* **1992**, *139*, 363–366.

[49] Masquelier, C.; Tabuchi, M.; Ado, K.; Kanno, R.; Kobayashi, Y.; Maki, Y.; Nakamura, O.; Goodenough, J. B. Chemical and Magnetic Characterization of Spinel Materials in the $LiMn_2O_4$–$Li_2Mn_4O_9$–$Li_4Mn_5O_{12}$ System. *J. Solid State Chem.* **1996**, *123*, 255 – 266.

[50] Sai Gautam, G.; Canepa, P.; Urban, A.; Bo, S.-H.; Ceder, G. Influence of Inversion on Mg Mobility and Electrochemistry in Spinels. *Chem. Mater.* **2017**, *29*, 7918–7930.

[51] Banerjee, S. K.; O'Reilly, W.; Gibb, T.; Greenwood, N. The behaviour of ferrous ions in iron-titanium spinels. *J. Phys. Chem. Sol.* **1967**, *28*, 1323 – 1335.

[52] Sickafus, K. E.; Wills, J. M.; Grimes, N. W. Structure of Spinel. *J. Am. Ceram. Soc.* **1999**, *82*, 3279–3292.

[53] Wheeler, E. M.; Lake, B.; Islam, A. T. M. N.; Reehuis, M.; Steffens, P.; Guidi, T.; Hill, A. H. Spin and orbital order in the vanadium spinel MgV_2O_4. *Phys. Rev. B* **2010**, *82*, 140406.

[54] Shannon, R. D. Revised effective ionic radii and systematic studies of interatomic distances in halides and chalcogenides. *Acta Cryst. A* **1976**, *32*, 751–767.

[55] Rouxel, J. Anion-Cation Redox Competition and the Formation of New Compounds in Highly Covalent Systems. *Chem. Eur. J.* **1996**, *2*, 1053–1059.

[56] Grimaud, A.; Hong, W. T.; Shao-Horn, Y.; Tarascon, J. M. Anionic redox processes for electrochemical devices. *Nat. Mater.* **2016**, *15*, 121–126.

[57] Emly, A.; Van der Ven, A. Mg Intercalation in Layered and Spinel Host Crystal Structures for Mg Batteries. *Inorg. Chem.* **2015**, *54*, 4394–4402.

[58] Lacroix, C.; Mendels, P.; Mila, F. *Introduction to Frustrated Magnetism: Materials, Experiments, Theory*; Springer Series in Solid-State Sciences; Springer Berlin Heidelberg, 2011.

[59] Patrie, M.; Domange, L.; Flahaut, J. Chimie minerale - sur une nouvelle serie de spinelles soufres contenant des terres rares ou du scandium. *C. R. Hebd. Seances Acad. Sci.* **1964**, *258*, 2585–2586.

[60] Guittard, M.; Souleau, C.; Farsam, H. Sur une nouvelle serie de spinelles selenies des terres rares de lyttrium et du scandium. *C. R. Hebd. Seances Acad. Sci.* **1964**, *259*, 2487–2489.

[61] Asahi, R.; Taga, Y.; Mannstadt, W.; Freeman, A. J. Electronic and optical properties of anatase TiO_2. *Phys. Rev. B* **2000**, *61*, 7459–7465.

[62] Ben Yahia, M.; Vergnet, J.; Saubanère, M.; Doublet, M.-L. Unified picture of anionic redox in Li/Na-ion batteries. *Nat. Mater.* **2019**, *18*, 496–502.

[63] Li, Z.; Vinayan, B. P.; Jankowski, P.; Njel, C.; Roy, A.; Vegge, T.; Maibach, J.; Lastra, J. M. G.; Fichtner, M.; Zhao-Karger, Z. Multi-Electron Reactions Enabled by Anion-Based Redox Chemistry for High-Energy Multivalent Rechargeable Batteries. *Angew. Chem. Int. Ed.* **2020**, *59*, 11483–11490.

[64] Tang, W.; Sanville, E.; Henkelman, G. A grid-based Bader analysis algorithm without lattice bias. *J. Phys.: Condens. Matter* **2009**, *21*, 084204.

[65] Dillenz, M.; Sotoudeh, M.; Euchner, H.; Groß, A. Screening of Charge Carrier Migration in the $MgSc_2Se_4$ Spinel Structure. *Front. Energy Res.* **2020**, *8*, 584654.

[66] Goldschmidt, V. M. Die Gesetze der Krystallochemie. *Naturwissenschaften* **1926**, *14*, 477.

[67] Goldschmidt, V. M. Crystal structure and chemical constitution. *Trans. Faraday Soc.* **1929**, *25*, 253–283.

[68] Stevanović, V.; d'Avezac, M.; Zunger, A. Simple Point-Ion Electrostatic Model Explains the Cation Distribution in Spinel Oxides. *Phys. Rev. Lett.* **2010**, *105*, 075501.

Figures

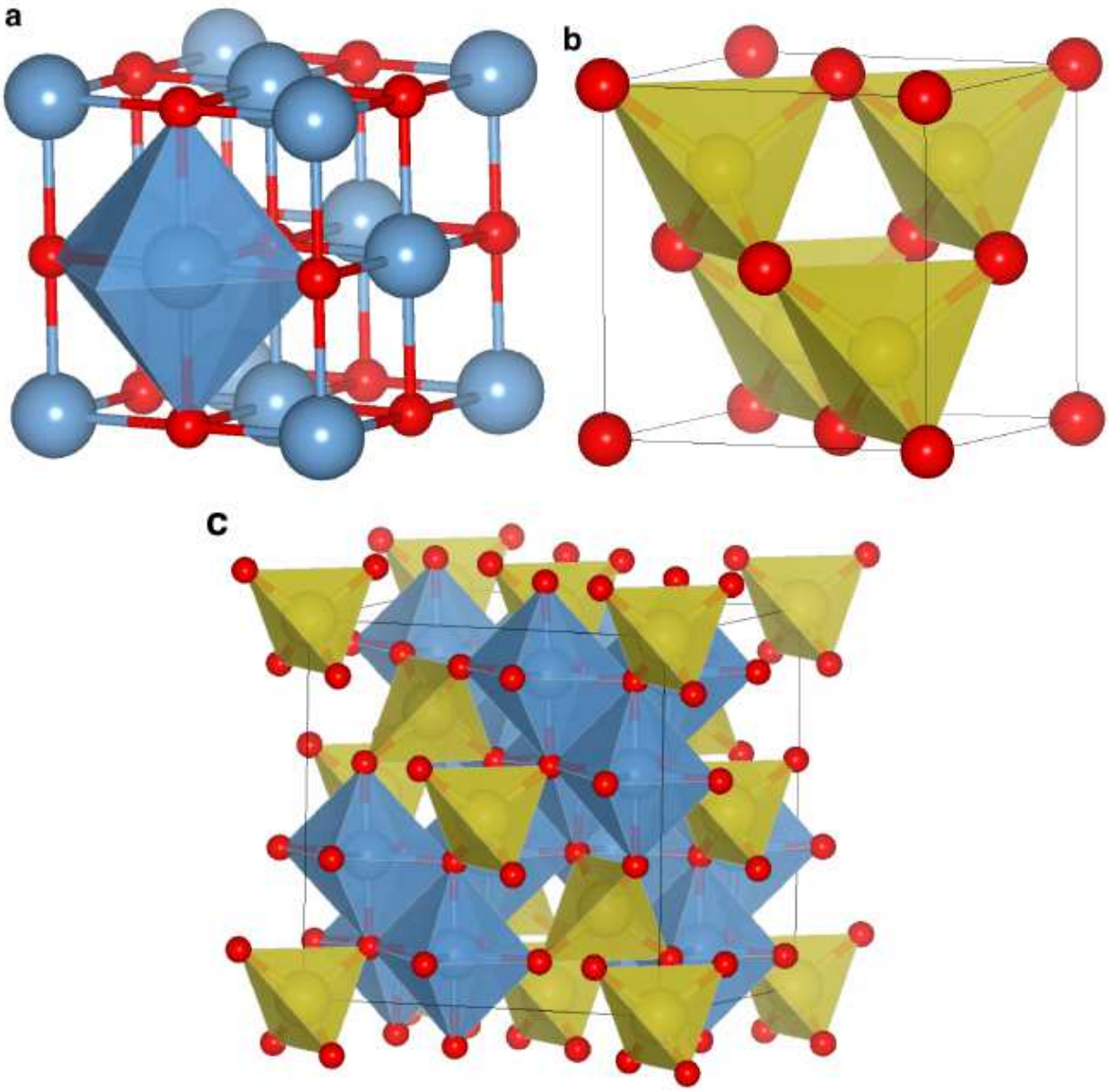

Figure 1

(a) Rock-salt, (b) zinc-blende, and (c) spinel structure. The spinel lattice is an ordered mixture of the zinc-blende and rock-salt structure. The A species (yellow) of AB2X4 occupy the tetrahedral sites, while the B species (blue) only occupy octahedral sites. The red spheres denote the oxide and chalcogenide anions such as O2-, S2-, and Se2-.

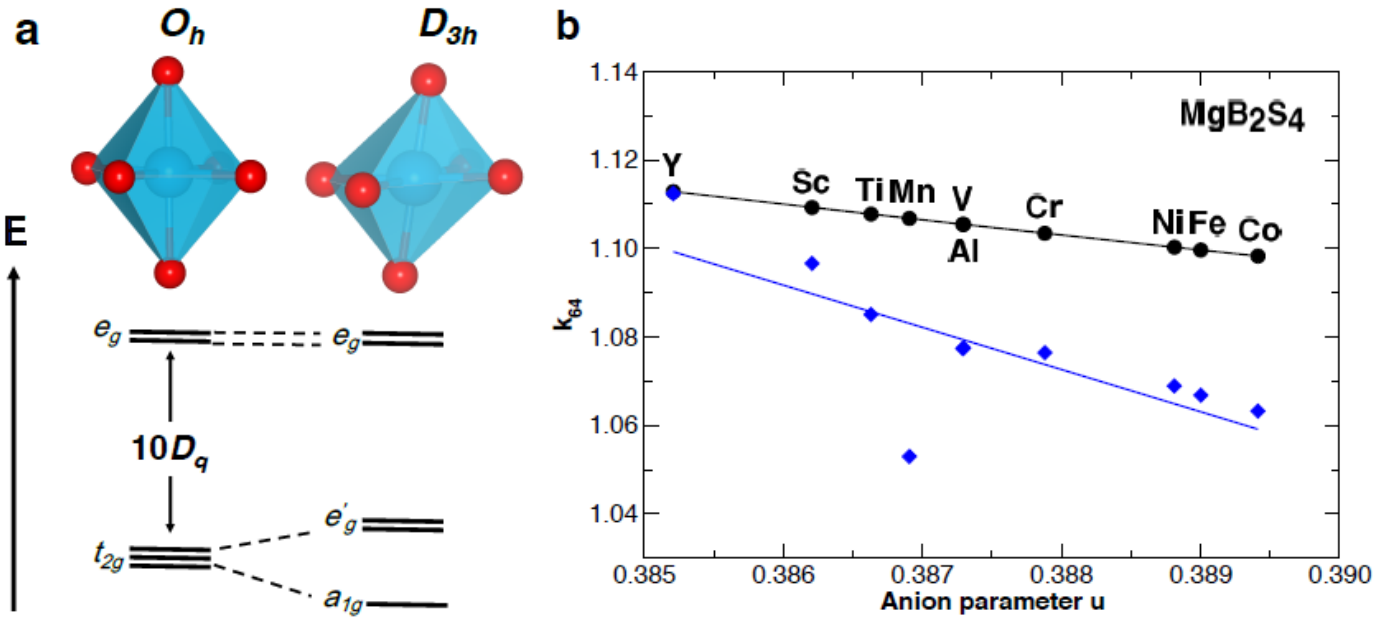

Figure 2

(a) Illustration of the transition from an undistorted octahedron cage with a Oh octahedral symmetry to a trigonally distorted cage with a D3h octahedral symmetry and the associated further crystal eld splitting of the d-states. (b) Dependence of the ratio k64 on the anion parameter u characterizing the trigonal distortion for S-spinels. The black dots denote the results for the original spinel structures with the Mg ion in a tetrahedral site and the octahedral vacancy being empty, and the black line corresponds to the analytical expression Eq. 5. The blue diamonds are determined for the relaxed spinels with the octahedral site occupied by a Mg anion. The blue line is a linear regression of these results. Note that the results for V and Al lie on top of each other for both considered cases.

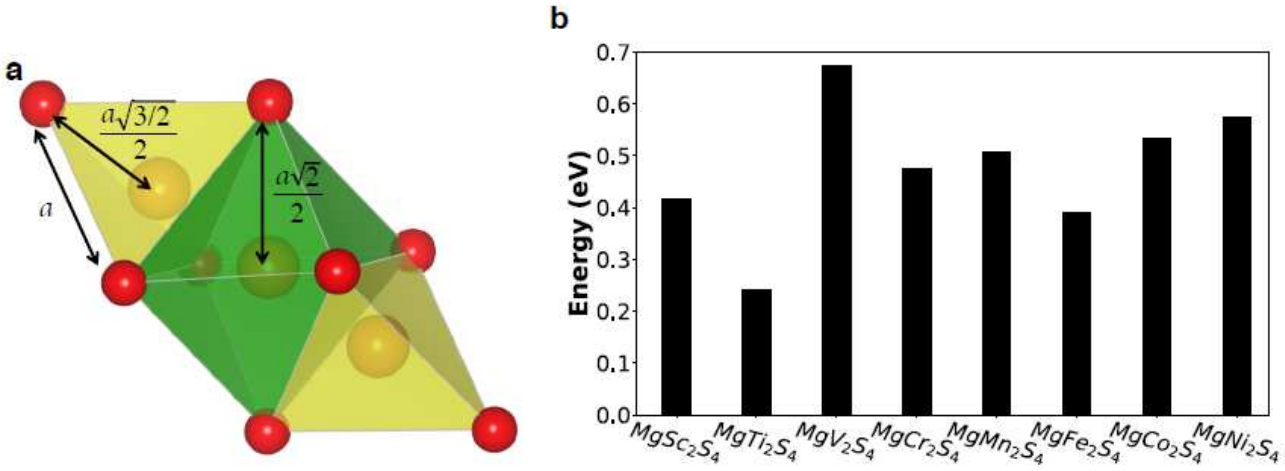

Figure 3

(a) Illustration of single-ion migration from tetrahedral site to the octahedral void and then to the next tetrahedral site. The chalcogenide atoms such as S and Se are shown by the red spheres, the migrating Mg ion is presented by the spheres inside the tetrahedrons and the octahedron. (b) Calculated Mg migration barriers for several transition metal ions in the sulfide-spinels.

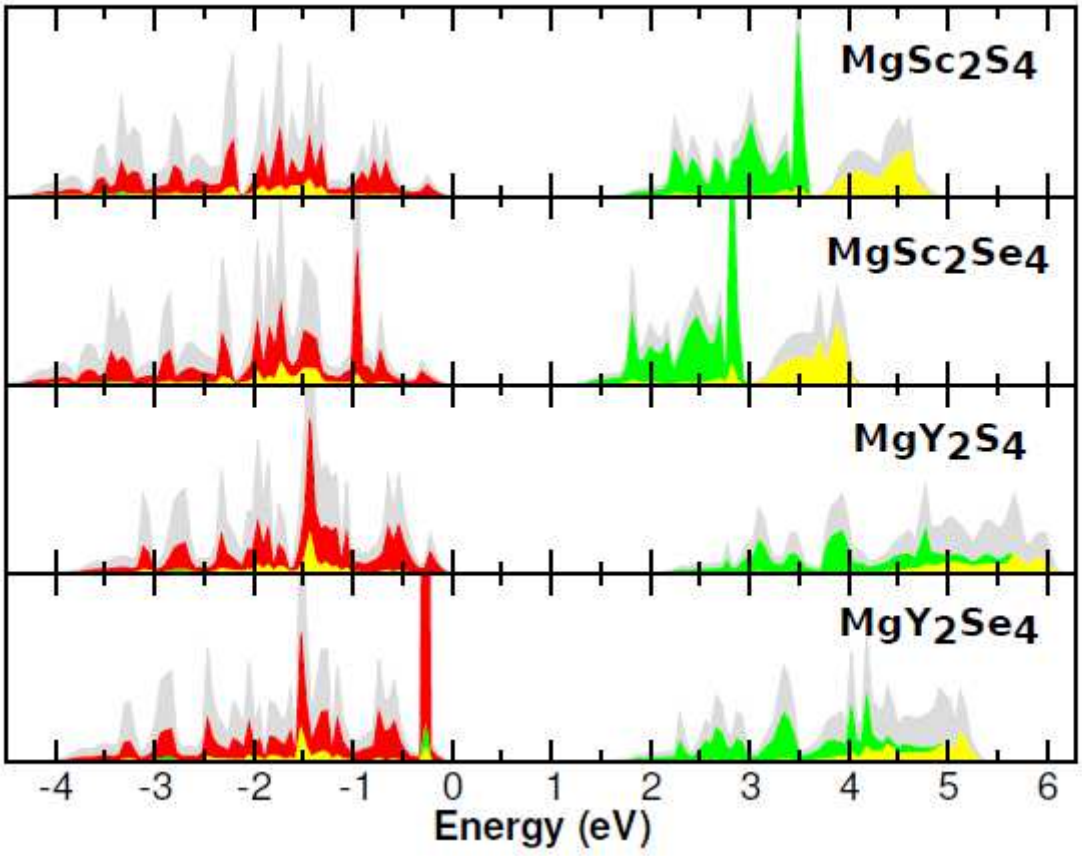

Figure 4

Density of states for MgSc2S4, MgSc2Se4, MgY2S4, and MgY2Se4 from top to bottom. The total DOS is given in gray. The projected DOS are shown in red for S and Se, in green for t2g and yellow for eg d-orbitals. The energy zero is set to the top of the valence band.

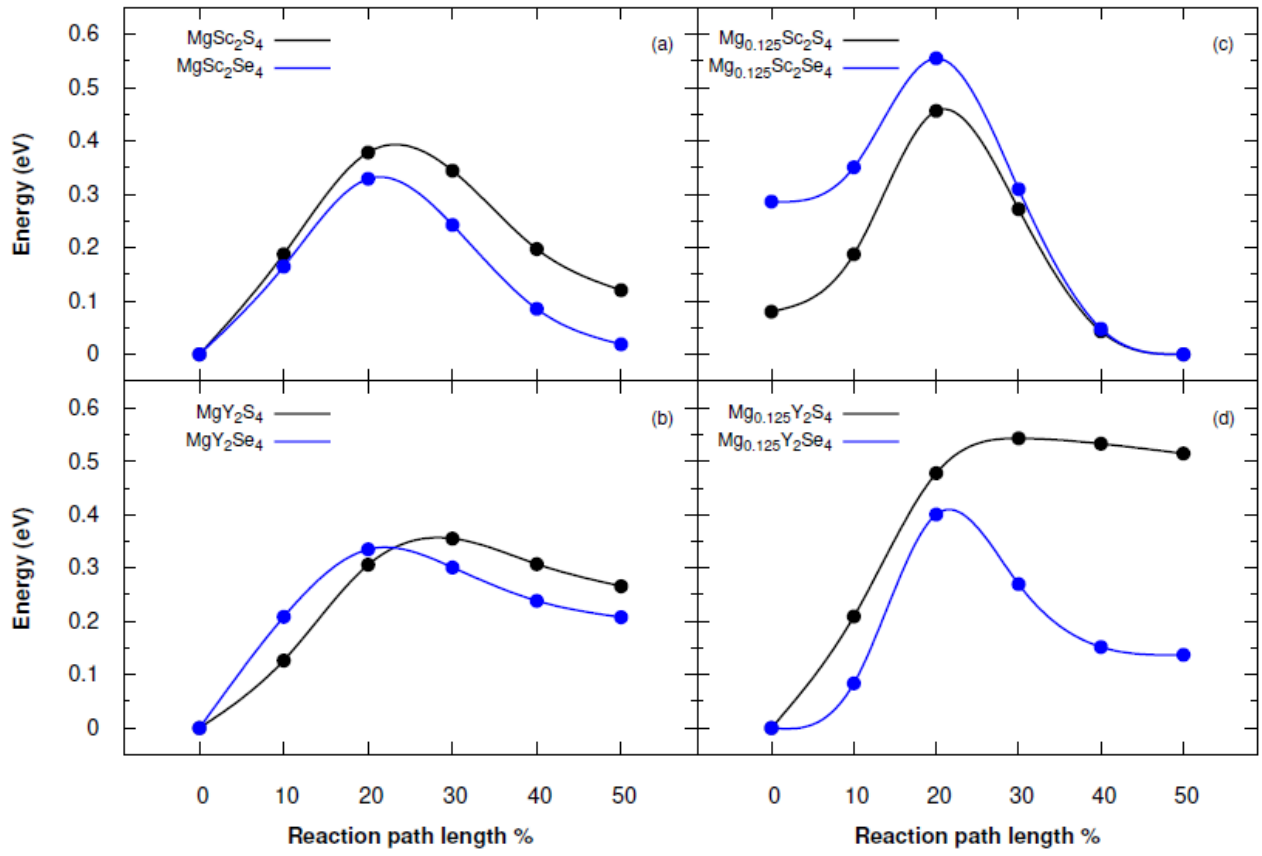

Figure 5

The Mg2+ migration energy barriers (in eV) as a function of the reaction path coordinate derived from periodic DFT calculations combined with NEB for the single-ion migration from tetrahedral site to the octahedral void corresponding to the S-spinels (black) and the Se-spinels (blue) for low and high concentrations of Mg ions. Note that the full migration path in principle includes the further migration from the octahedral to the tetrahedral site, but as the corresponding energies are symmetric with respect to the octahedral site, this part is omitted.

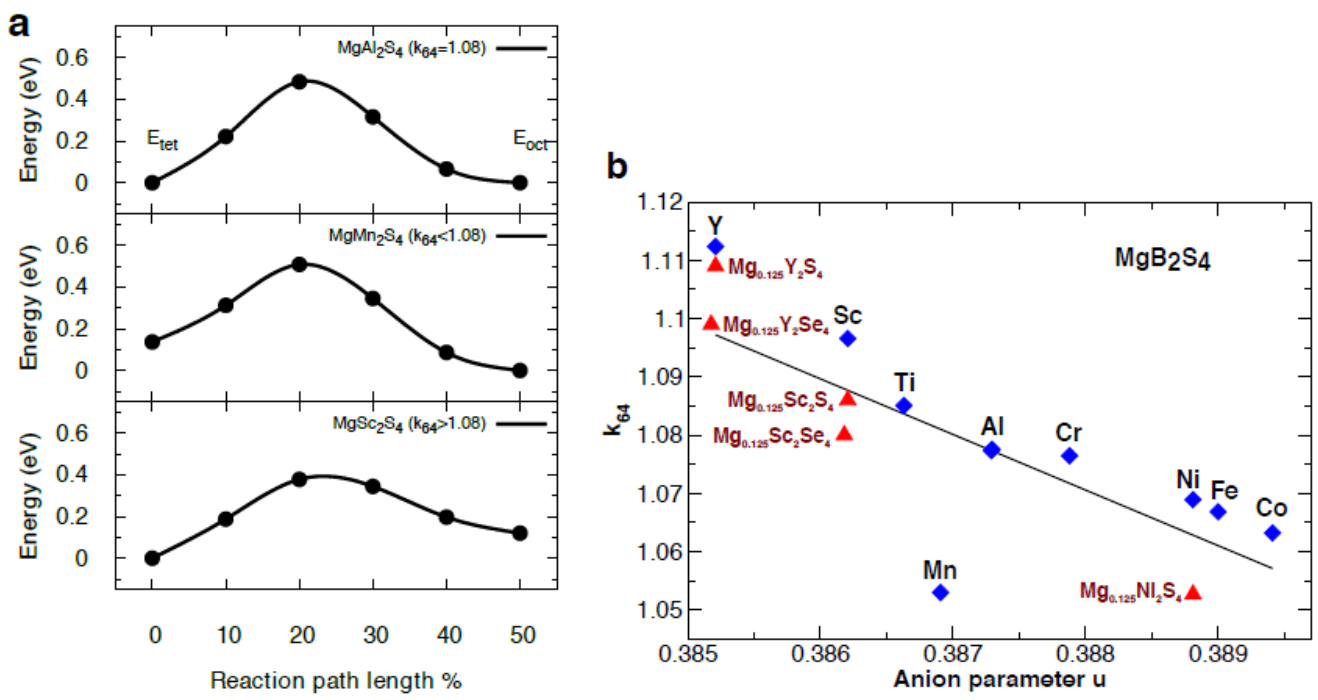

Figure 6

a) Mg-ion migration barriers for spinel compounds with different trigonal distortions characterized by k64. (b) The ratio k64 as a function of the anion parameter u for selected spinel compounds. Blue diamonds denote high Mg concentration compounds and red triangles low Mg concentration compounds. The black line represents a dividing line between Mg tetrahedral and octahedral site preference.